

# The Effects of Photon Spectrum and Variable Thermal Conductivity on the Distribution of Temperature in an Inclined Plate Crotch Absorber

## 1 INTRODUCTION

Absorption of photons in a metal is varied up to the photon energy spectrum. For example, larger wavelength photons generally can be more easily absorbed when they pass through an absorber while shorter ones tend to penetrate. This spectral variation of photon energy absorption takes place angularly due to the angular variation of the synchrotron radiation power. In this note, the effects of photon spectrum have been investigated for the thermal analysis of crotch absorbers. In addition, the effects of variable thermal conductivity have also been investigated. The heat generation due to the photon energy deposition diffuses throughout the metal with the thermal conductivity  $k$  which is dependent on the temperature field. This temperature dependence of the conductivity results in a non-linear heat conduction equation. This note presents both effects of the photon spectrum and the variable thermal conductivity on the temperature distribution for inclined crotch absorbers. A finite difference program was written and the calculation results were compared with the previous analytical solution[1] which assumed constant conductivity and absorption coefficient.

## 2 ANALYSIS

### 2.1 Governing Equations

The governing heat conduction equation with heat generation may be written for the variable thermal conductivity as;

$$\nabla \cdot (k(T)\nabla T) = -f(x, y) \quad (1)$$

where  $k(T)$  is the thermal conductivity which is a function of temperature  $T$ . In the above equation, the heat generation,  $f(x, y)$ , may be written for a vertically inclined plate with angle  $\theta$  as

$$f(x, y) = \int_0^\infty \alpha_\lambda I_o(-x\cos\theta + (y - b/2)\sin\theta, \lambda) \cdot \exp(-\alpha_\lambda \frac{x}{\sin\theta}) d\lambda \quad (2)$$

where  $I_o$ ,  $\alpha_\lambda$  and  $\lambda$  are the incident synchrotron radiation power density, the absorption coefficient of the metal and the wavelength of photon, respectively. Spectral and angular distribution of the incident bending magnet radiation,  $I_o$ , is given by;

$$I_o(\psi = y'/l, \lambda) = \frac{P_d}{l^2} \quad (3)$$

$$= 7.569 \cdot 10^{14} \frac{IE^6 B^2}{l^2} \left(\frac{\lambda_c}{\lambda}\right)^4 F\left(\frac{\lambda_c}{2\lambda}, \gamma\psi\right) [W/m^2 rad\psi]$$

where  $F$  has vertical and parallel polarized components which are given in [2];

$$F = F_{\parallel} + F_{\perp}$$

$$F_{\parallel} = (1 + (\gamma\psi)^2)^2 K_{2/3}^2 \left[\frac{\lambda_c}{2\lambda} (1 + (\gamma\psi)^2)^{3/2}\right]$$

$$F_{\perp} = \gamma^2 \psi^2 (1 + (\gamma\psi)^2) K_{1/3}^2 \left[\frac{\lambda_c}{2\lambda} (1 + (\gamma\psi)^2)^{3/2}\right]$$

where  $E$ ,  $I$ ,  $B$ ,  $l$ ,  $\lambda_c$ ,  $\gamma$  and  $K$  are the positron energy in  $GeV$ , the positron beam current in  $mA$ , the magnetic field of bending magnet in  $T$ , the tangential length from the source to the plate in  $m$ , the critical wave length which is equal to  $\frac{4\pi\rho}{3\gamma^3} = \frac{4\pi \cdot 3.335E}{3\gamma^3 B}$ ,  $\gamma = \frac{E}{m_0 c^2} = 1957E$  and the modified bessel function, respectively. Utilizing the change of variable in equation (2) from  $\lambda$  to  $\eta = \frac{\lambda_c}{\lambda} = \frac{e}{e_c}$  and substituting equation (3) into equation (2) yield:

$$f(x, y) = \frac{1.4107 \cdot 10^3 E^4 B I}{l^2} \cdot \int_0^\infty \alpha_\lambda \eta^2 F(\eta, \gamma\psi) \cdot \exp\left(-\alpha_\lambda \frac{x}{\sin\theta}\right) d\eta \quad (4)$$

where  $e$  and  $e_c$  are photon energy and critical photon energy, respectively.

The absorption coefficient  $\alpha_\lambda$  in equation (4) is dependent on photon energy. For photon energies above 1 KeV and less than 1000 KeV,  $\alpha_\lambda$  was evaluated using the following least square fitting formula taht was derived from the data in [3]:

$$\log_{10}(\alpha_\lambda) = \sum_i a_i (\log_{10} e)^i \quad (5)$$

where  $a_i$ 's are given in Table (1) for copper and beryllium. For photon energies less than 1 KeV, data given in [3] were used. The contribution of photon energies less than 0.1 KeV

or greater than 1000 KeV was calculated and found to be negligible compared to the total power density.

Variable thermal conductivities in equation (1) were calculated using a polynomial fitting formula:

$$k(T) = \sum_i b_i T^i \quad (6)$$

and coefficients  $b_i$  are given in Table (1) for copper and beryllium.

## 2.2 Numerical Program

A finite difference program was written to solve the two dimensional heat conduction problem with the distributed heat generation. This program uses a non-uniform grid system as shown in Figure (1-1). Boundary conditions and geometry are given in Fig.(1-1). Note that the photon penetration with tilted angle requires to solve the full domain from  $y=-b/2$  to  $y=b/2$ . If a vertical plate case ( $\theta = 90$  degree) is considered, only half domain for  $y > 0$  is needed to solve since the temperature fields are symmetric with respect to the center line through  $y = 0$ . Figure (1-2) shows the typical internal control volume in which energy balance condition yields the following difference equation:

$$a_P T_P = a_E T_E + a_W T_W + a_N T_N + a_S T_S + b \quad (7)$$

where

$$a_E = k_e \frac{sn_s}{x(E) - x(P)}, \quad a_W = k_w \frac{sn_s}{x(P) - x(W)}$$

$$a_N = k_n \frac{se_w}{y(N) - y(P)}, \quad a_S = k_s \frac{se_w}{y(P) - y(S)}$$

$$b = f_P \cdot se_w \cdot sn_s, \quad a_P = a_E + a_W + a_N + a_S$$

$$k_e = \frac{k_E + k_p}{2}, \quad k_w = \frac{k_W + k_p}{2}$$

$$k_n = \frac{k_N + k_p}{2}, \quad k_s = \frac{k_S + k_p}{2}$$

$$sn_s = \frac{y(N) - y(S)}{2}, \quad se_w = \frac{x(E) - x(W)}{2}$$

The surfaces of the control volume locate at the centers of the two adjacent nodal points. The heat generation term  $f_P$  was calculated integrating equation (2) along with equations (3), (4) and (5) numerically. For a grid system (M,N), the above difference equation sets  $M * N$  linear algebraic equations for  $M * N$  unknown T's. Line by line iteration along with TDMA(Tri-Diagonal Matrix Algorithm)[4] was used to solve the above difference equations. The convergence criteria was chosen so that the numerical results are assumed to be converged when the residual of the above difference equation becomes less than 0.001. Grid sensitivity tests were done to find the appropriate grid size which produces reasonable grid independent results. The grid of (60,71) was used for beryllium plate calculations and (65,81) for Cu plates.

### 3 RESULTS AND DISCUSSION

In this section, the confirmation of the present numerical program comparing its results with the previous analytical solution will be presented first and the effects of photon spectrum and variable thermal conductivity will then be discussed.

Figure (2) shows the comparison of the present numerical results with the analytical results[1]. Solid lines designate temperatures obtained by the present numerical solution and solid circles are from the previous analytical solution results. X-axis of the figure corresponds to either dimensionless coordinate  $X = \frac{x}{a}$  or  $Y = \frac{y+b/2}{b/2}$ . For both analyses, the same values of the constant thermal conductivity and the absorption coefficient were used to confirm the numerical program. It is shown that two results are in very good agreement. It is noted that when the constant absorption coefficient is used, the equation (4) can be simplified using the following approximation[2]:

$$\int_0^{\infty} I_o(y', \lambda) d\lambda = \int_0^{\infty} \frac{P(y', \lambda)}{l^2} d\lambda$$

$$\approx \frac{12.4E^4 BI}{l^2} \cdot 0.4375 \exp\left(-\left(\frac{\gamma y'}{0.608l}\right)^2 / 2\right) [kw/m^2]$$

The above approximation utilized in the previous analytical study was shown to be in good agreement with the results obtained by the direct numerical integration of equation (4), which is shown in Figure (3).

Figure (4) shows the effects of photon spectrum on the temperature distribution in a vertical crotch absorber . Solid lines are numerical results which include variable absorption coefficients  $\alpha_\lambda$  that depends on the photon spectrum while circles and rectangles are analytical ones using the assumption of the constant values of  $\alpha_\lambda$ . For the analytical solution, two cases were considered; i.e. in Fig.(4) circles are for  $\alpha_\lambda = 53.02$  [1/m] corresponding to the photon energy that has the maximum power density and rectangles are for  $\alpha_\lambda = 43.3$  [1/m] corresponding to the critical energy. Figure (5-1) shows dimensionless bending magnet radiation power density with respect to  $\eta = \frac{e}{e_c}$  and  $\gamma\psi$  ( refer to the function  $\eta^2 F$  in the integrand of equation (4) ). It is noted that the maximum occurs at  $\psi = 0$  and as  $\psi$  increases, the maximum point in the constant  $\gamma\psi$  plane moves to the lower energy. This trend is more clearly shown in Figure (5-2) which also shows that the maximum dimensionless power density per unit  $\eta$  (dimensionless photon energy) occurs near  $e = e_c$ . This point was found to be at  $\frac{e}{e_c} = 0.8337$  solving  $\frac{d(\eta^2 F(\eta, \psi=0))}{d\eta} = 0$ . It is seen in Figures (4) that the assumption of constant values of absorption coefficient underestimate photon energy deposition near surface( at  $x=0$  ) and overestimate at the depth of the plate and  $\alpha_\lambda$  corresponding to the maximum power density ( circles ) seems to yield better agreement with the numerical solution than the one corresponding to the critical energy ( rectangles ). Figure (6) is the case of inclined plate with  $\theta = 50$  which shows the same trend, i.e. the use of  $\alpha_\lambda$  for the maximum power density resulted in better results. Note that Fig. 6 shows the asymmetric temperature distribution with respect to  $Y = 0.5$  at the center of the plate ( note that in Fig.(2) for a vertical plate the temperature distribution is symmetric ).

Figure (7) shows the effects of the variable thermal conductivity for an inclined Be plate with  $\theta = 50$ . All cases in Fig.(7) were obtained using numerical program which includes the effect of photon spectrum. Solid line is for variable conductivity, solid-dot, dotted and dashed ones are for constant conductivity with  $k = 140$  at  $T = 500K$  [5],  $k = 161$  at  $T = 400K$  [5] and  $k = 185$  used in [6], respectively. The solid-dot curve (  $k = 140$  that was evaluated at  $T=500$  K which was roughly the average of the maximum and minimum temperatures ) yielded best agreement with the variable conductivity case ( solid curve ).

For an inclined Cu plate, figure (8) shows the effects of the photon spectrum and the variable thermal conductivity. Solid curve is the case for both variable absorption coefficient and thermal conductivity, dashed one for the variable absorption coefficient but the constant conductivity and dotted one for both constant absorption coefficient and conductivity. It is

shown that for a Cu plate, constant  $k$  case agrees very well with variable  $k$  ( see solid and dashed curves) and even both constant absorption coefficient and conductivity case gives good agreement ( solid and dotted curves ).

In summary, a finite difference program was written to study the effects of the photon spectrum of bending magnet and the variable thermal conductivity on photon penetration heating for inclined plate absorbers. The present numerical results were compared with the previous analytical solution and the following conclusions were obtained.

For a Cu plate, constant conductivity and absorption coefficient yielded good agreement with the case that includes both photon spectrum and variable conductivity, which signifies that the effects of photon spectrum and variable thermal conductivity for copper absorbers are small and may be neglected. For a Be plate, there is about 10-25 % disagreement among cases of constant and variable absorption coefficients and constant and variable thermal conductivities and the evaluation of constant thermal conductivity at the average of the maximum and minimum temperatures along with the use of the constant absorption coefficient corresponding to the maximum power density was shown to minimize disagreement.

## REFERENCES

- [1] M. Choi, "A Note on Thermal Analysis for an Inclined Plate Crotch Absorber", ANL Light Source Note, June, 1989
- [2] G.K. Green, "Spectra and Optics of Synchrotron Radiation", BNL Report 50522
- [3] Wm.J. Veigele, "Photon Cross Sections from 0.1 KeV to 1 MeV for Elements Z=1 to Z=94", Atomic Data Tables, 5, 51-111, 1973
- [4] S.V. Patankar, "Numerical Heat Transfer and Fluid Flow", McGraw-Hill, New York, 1980
- [5] Y.S. Touloukian, R.W. Powell, C.Y. Ho and P.G. Klemens, "Thermal Conductivity Metallic Elements and Alloys", IFI/Plenum, New York, 1970
- [6] D.M. Mills, D.H. Bilderback and B.W. Batterman, "Thermal Design of Synchrotron Radiation Ports at CESR", IEEE Transactions on Nuclear Science, Vol. NS-26, No.3, pp. 3854-3856, 1979

Table (1) Coefficients of Fitting Formula of Equations (5) and (6)

<i>i</i>	<i>beryllium</i>		<i>copper</i>		
	$a_i$	$b_i$	$a_i$ for $e \leq 8.979$ eV	$a_i$ for $e > 8.979$ eV	$b_i$
1	3.9645	675.88	6.1212	22.7052	428.3
2	-1.9270	-3.1396	-2.1623	-59.9269	-0.1422
3	-12.5069	7.2436e-3	-1.1047	83.5454	1.6862e-4
4	52.3422	-7.8161e-6	0.6729	-61.9478	-9.8724e-8
5	-112.4062	3.1970e-9		24.4923	
6	137.73			-4.8904	

$a_7=-101.2312$ ,  $a_8=45.8069$ ,  $a_9=-12.623$ ,  $a_{10}=1.9844$ ,  $a_{11}=-0.148$  and  $a_{12}=2.5695e-3$  for *beryllium*

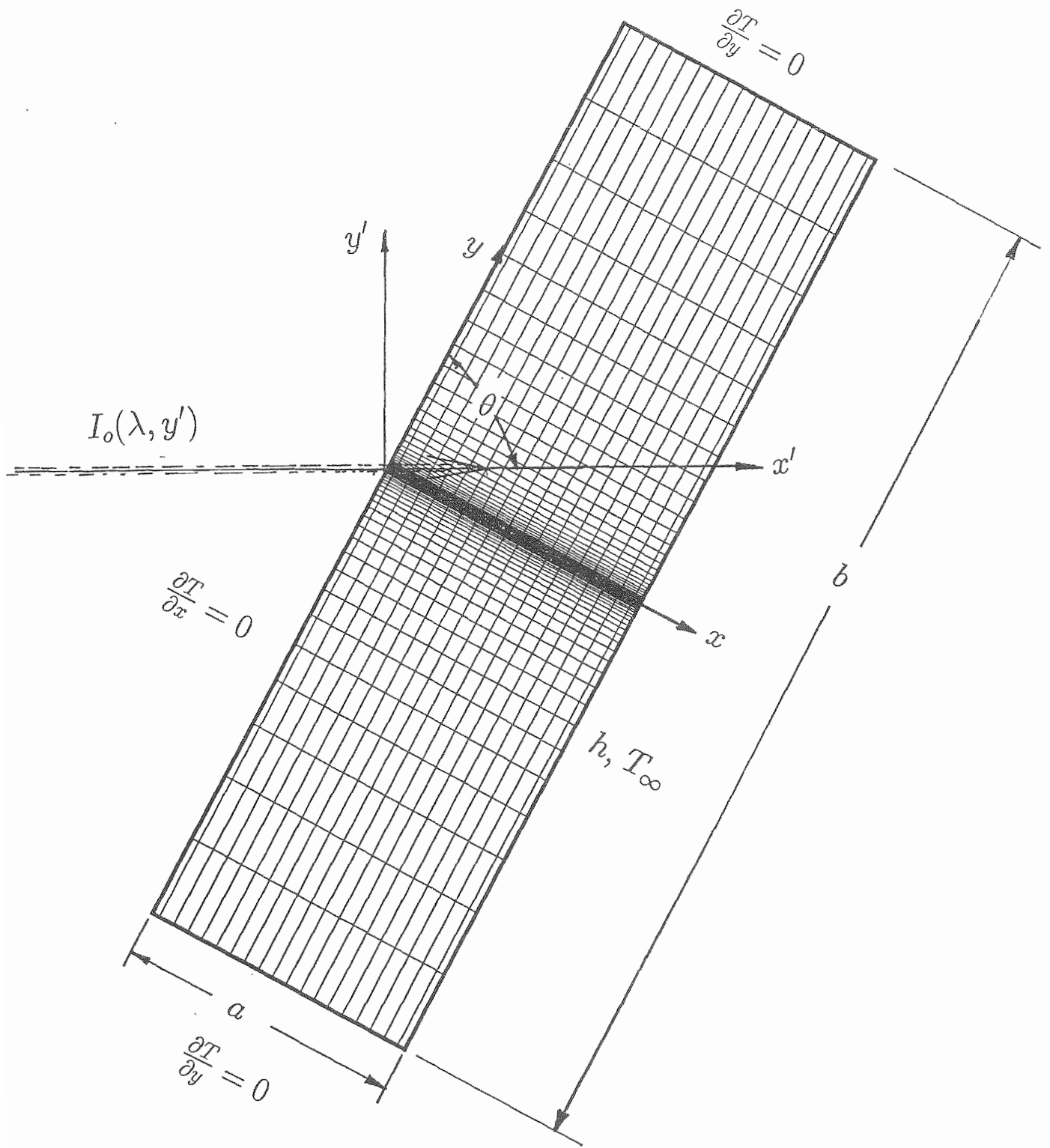


Figure (1-1) Geometry, Grid System\* and Boundary Conditions

\* This grid system doesn't represent the actual grid sizes, which were determined to result in a reasonably grid-independent solution.

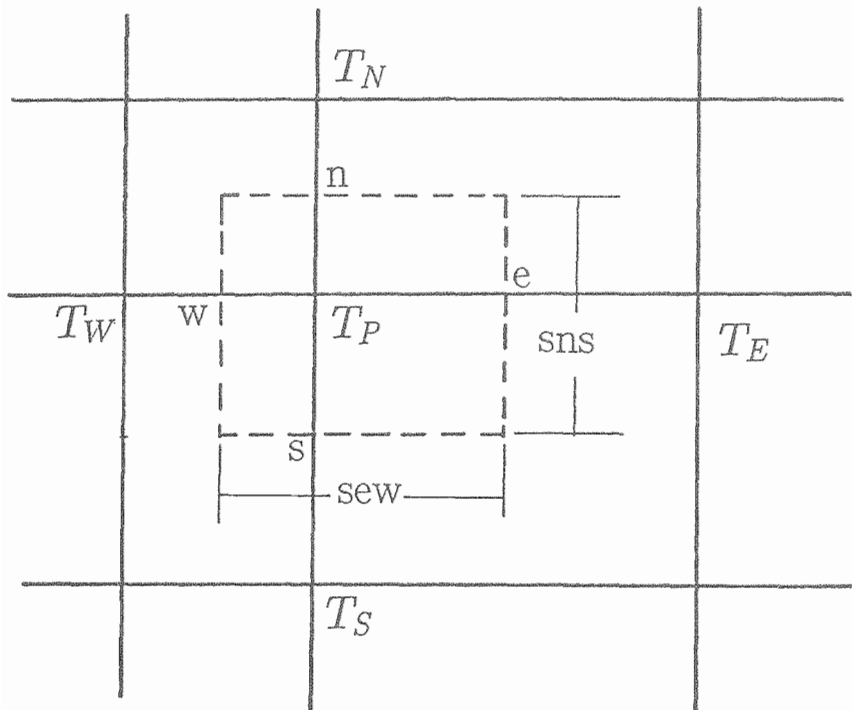


Figure (1-2) Schematic of a Typical Node Arrangement

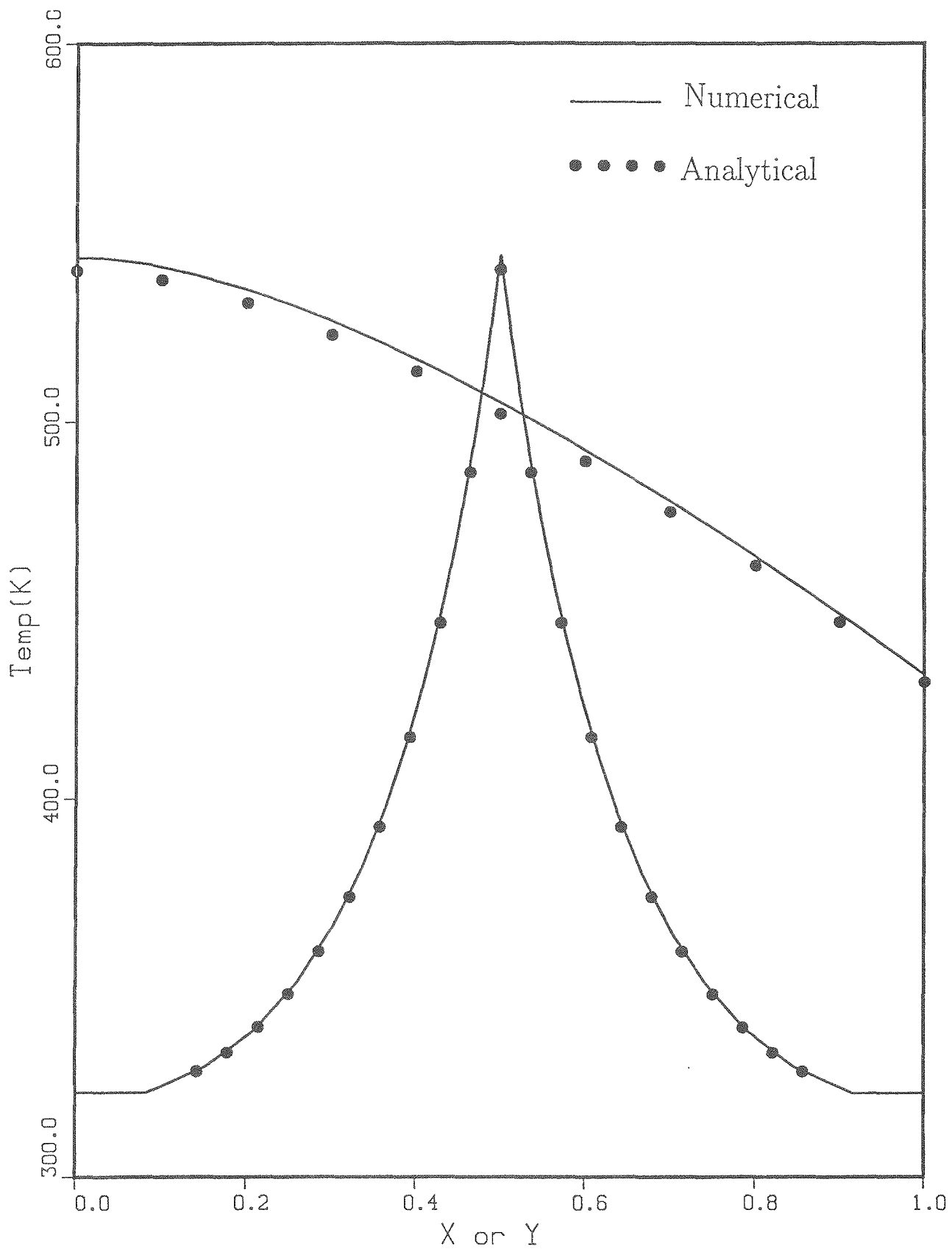


Figure (2) Comparison of the Present Numerical Results with the Previous Analytical Solution; Vertical *Be* Plate,  $a=2$  cm,  $b=14$  cm,  $\alpha_\lambda=43.3$  /m,  $h=12000$  W/m<sup>2</sup> K

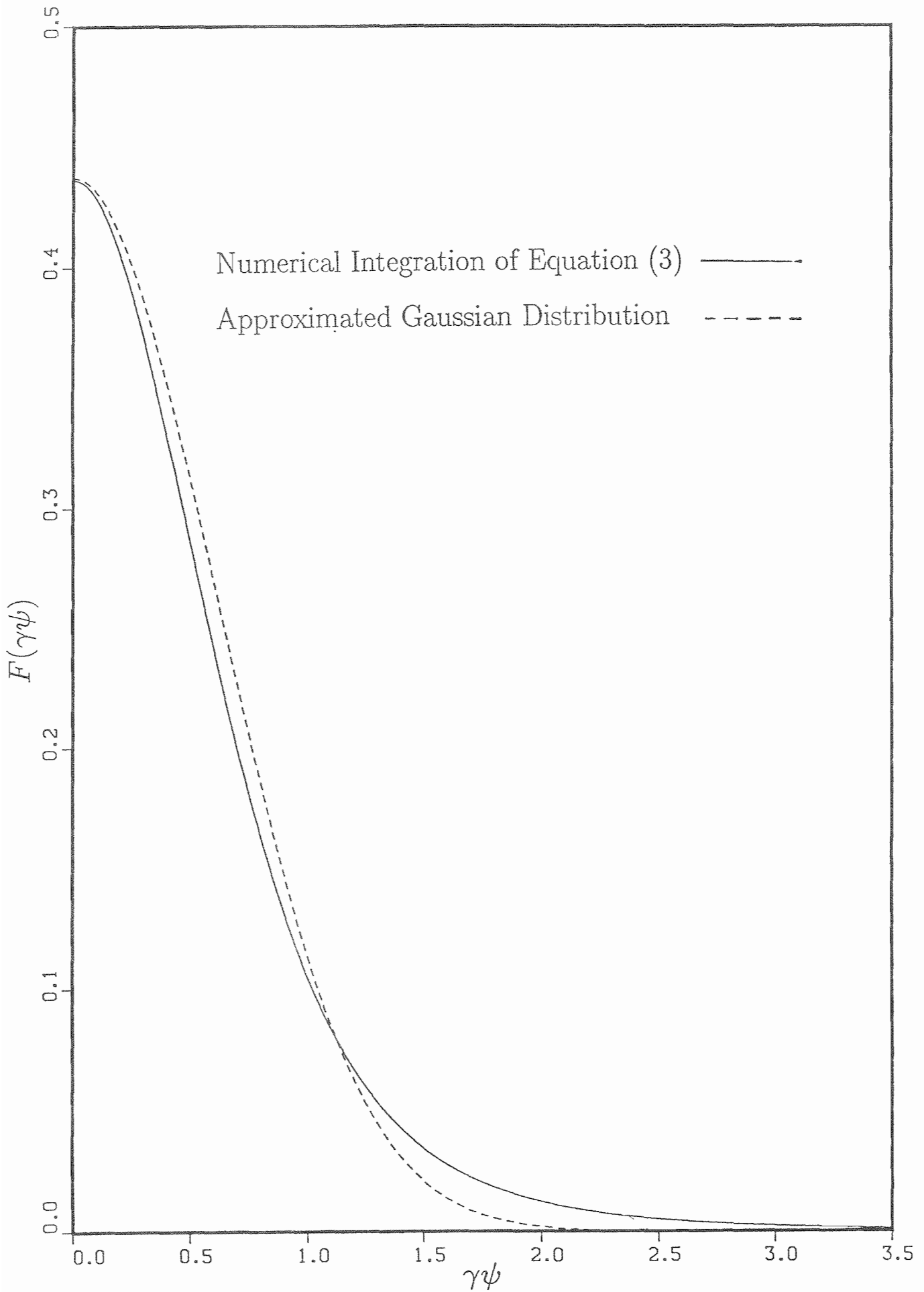


Figure (3) Angular Distribution of the Incident Total Radiation

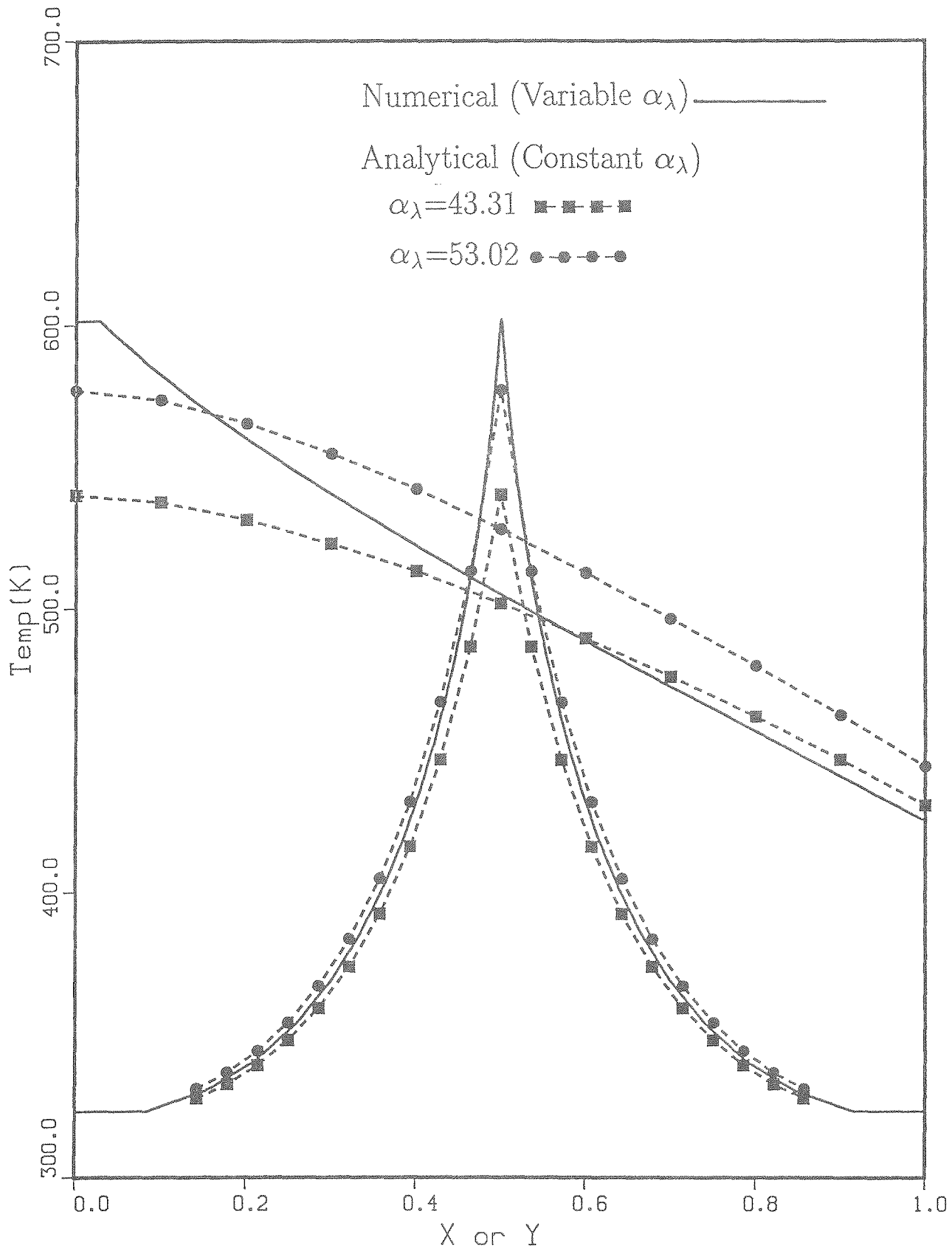


Figure (4) Effects of Photon Spectrum on the Temperature Distribution in a Vertical Be Plate ;  $a=2$  cm,  $b=14$  cm,  $h=12000$  W/m<sup>2</sup> K

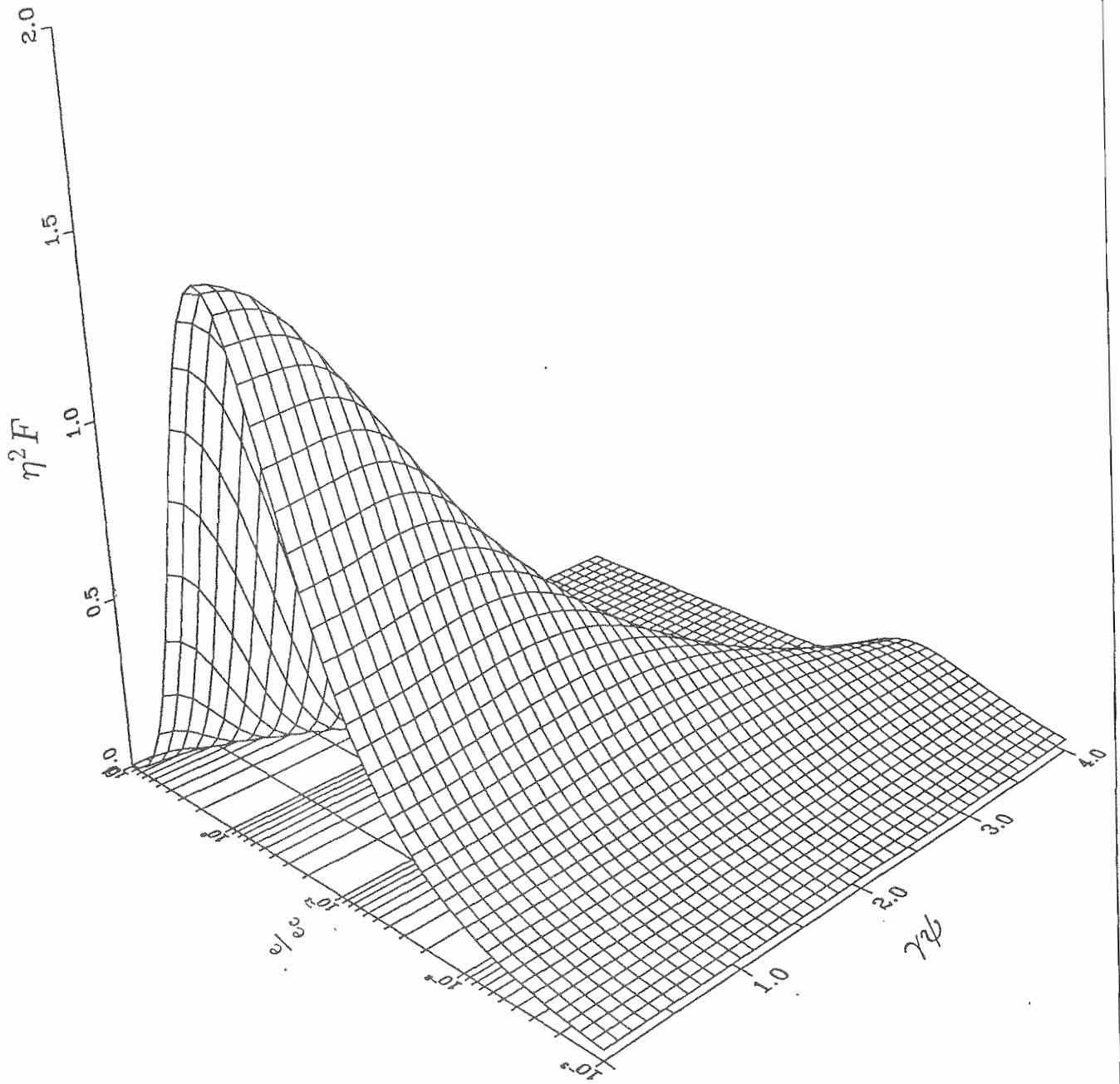


Figure (5-1) Spectral and Angular Distribution of Dimensionless Bending Magnet Radiation Power Density per Unit  $\eta$

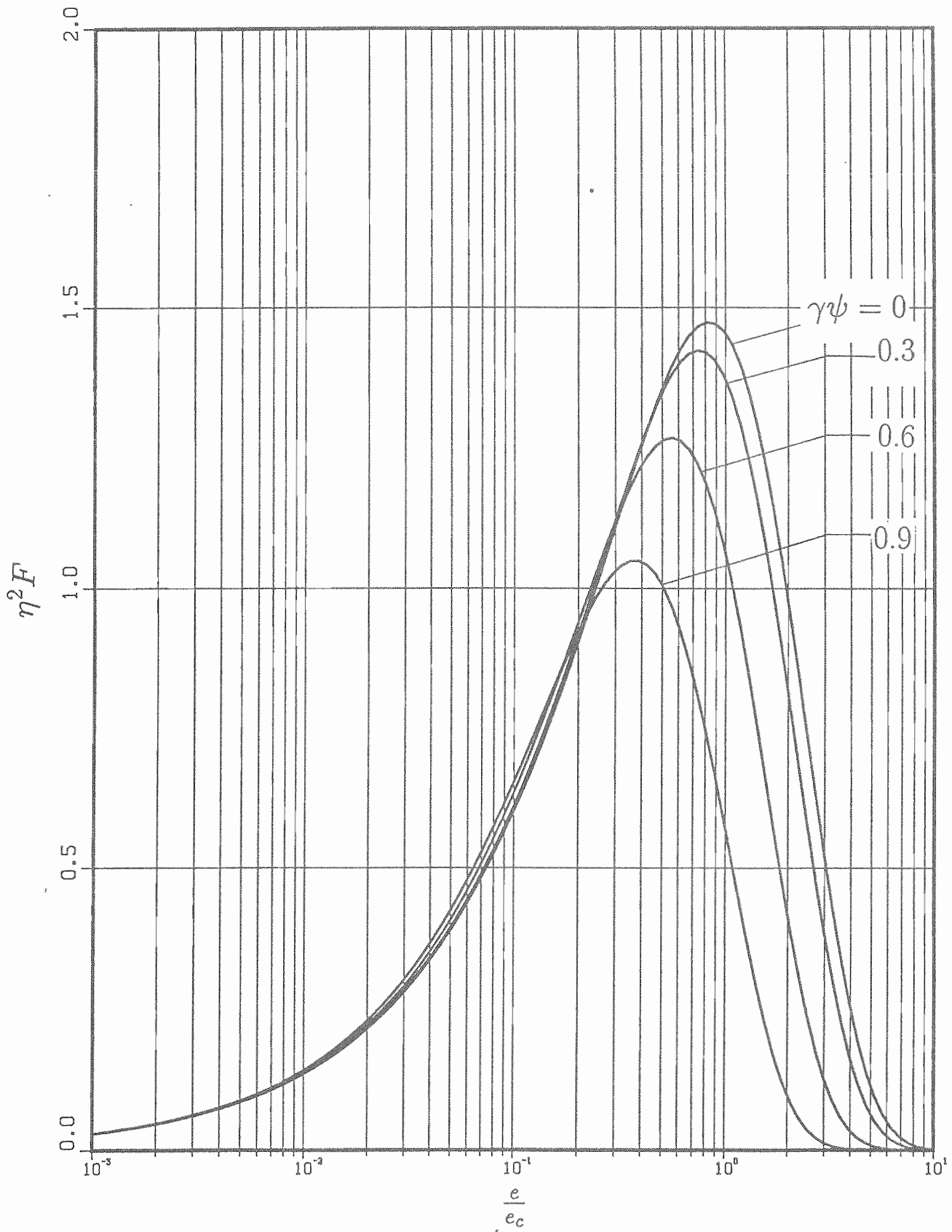


Figure (5-2) Spectral Variation of Dimensionless Bending Magnet Radiation Power Density per Unit  $\eta$  for Different Angular Locations

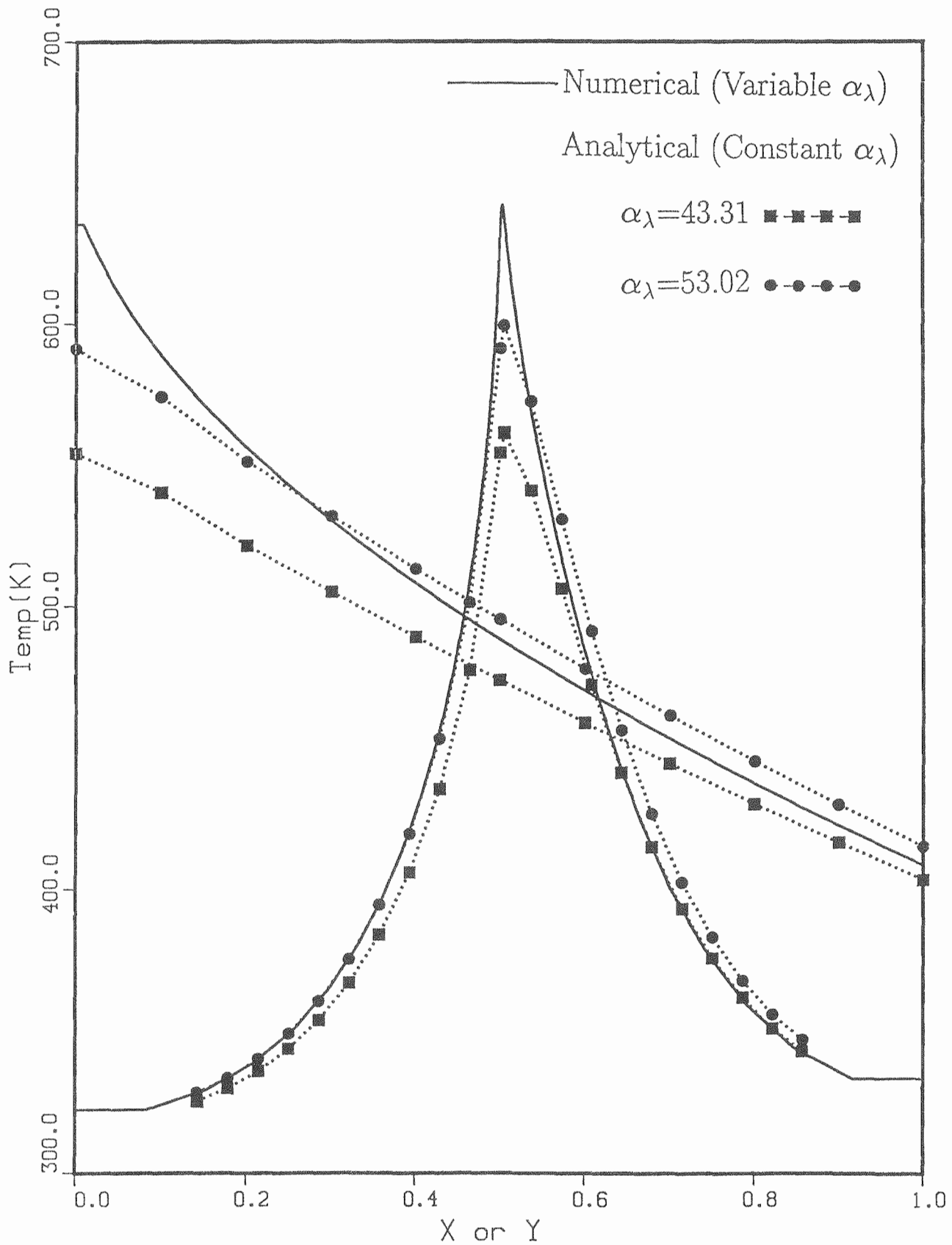


Figure (6) Effects of Photon Spectrum on the Temperature Distribution in an Inclined *Be* Plate with  $\theta = 50^\circ$

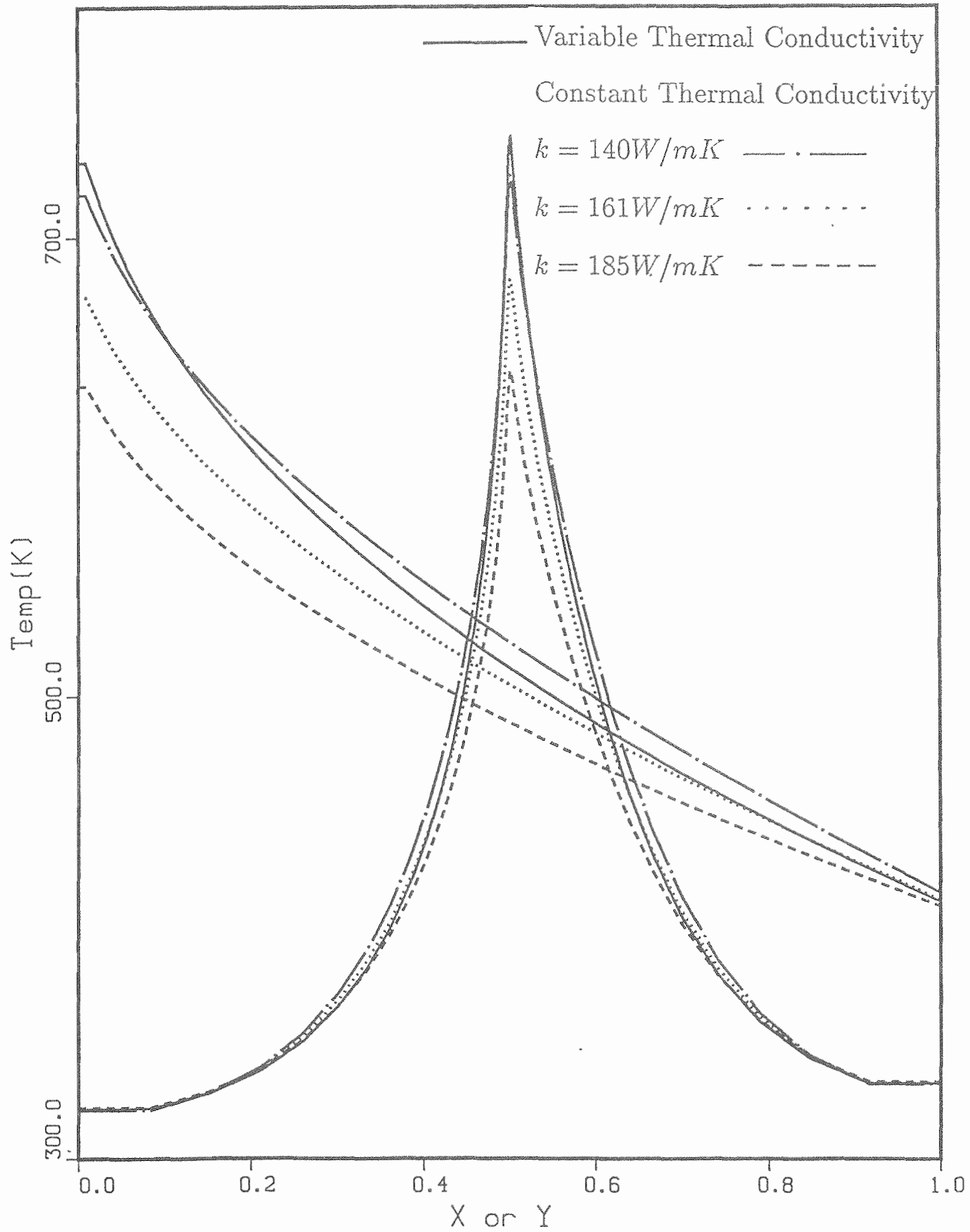


Figure (7) Effect of the Variable Thermal Conductivity for an Inclined *Be* Plate Crotch Absorber with  $\theta = 50^\circ$ ;  $a=2$  cm,  $b=14$  cm

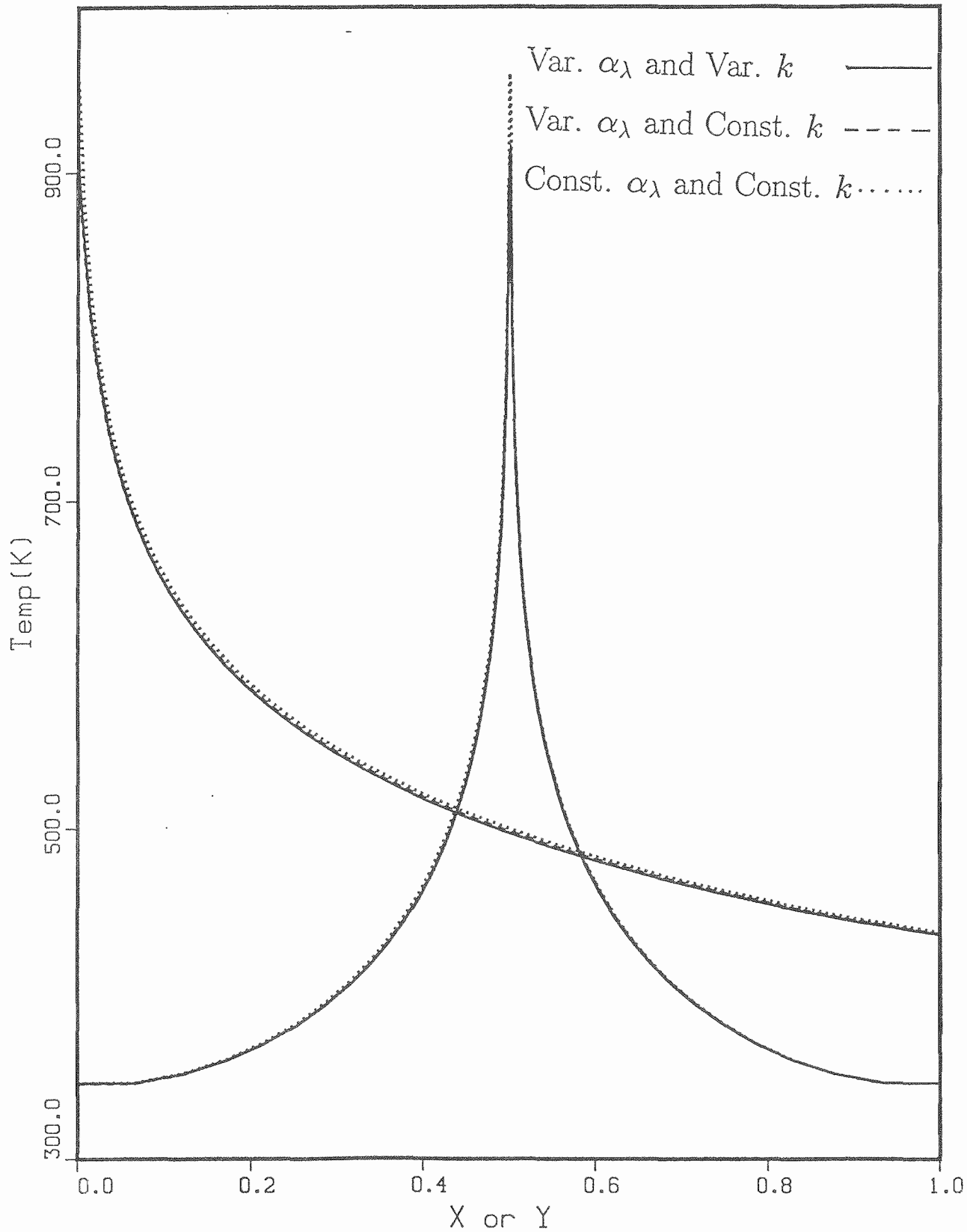


Figure (8) Effects of Photon Spectrum and Variable Thermal Conductivity for an Inclined *Cu* Plate with  $\theta = 50^\circ$ ;  $a=2$  cm,  $b=14$  cm